# Variational Scaling Law for Atmospheric Propagation

SOPHIA POTOCZAK BRAGDON[1,*], DANIEL CARGILL[2], AND JACOB GROSEK[3]

[1] Mathematics Department, Colorado State University, 1874 Campus Delivery, Fort Collins, CO 80523
[2] Lockheed Martin Corporation, 199 Borton Landing Road, Moorestown, NJ 08057
[3] Air Force Research Laboratory, Directed Energy Directorate, 3550 Aberdeen Ave SE, Albuquerque, NM 87117
[*] Corresponding author's email: potoczak@math.colostate.edu

Compiled October 9, 2020

**A new scaling law model for propagation of optical beams through atmospheric turbulence is presented and compared to a common scalar stochastic waveoptics technique. This methodology tracks the evolution of the important beam wavefront and phasefront parameters of a propagating Gaussian-shaped laser field as it moves through atmospheric turbulence, assuming a conservation of power. As with other scaling laws, this variational technique makes multiple simplifying assumptions about the optical beam in order to capture the essential features of interest, while significantly reducing the computational cost of calculation. This variational scaling law is shown to reliably work with moderately high turbulence strengths, producing at least a $\sim 2$x computational speed-up per individual propagation of the beam and $> 100$x memory reduction (depending on the chosen resolution).** 

http://dx.doi.org/10.1364/ao.XX.XXXXXX

## INTRODUCTION

The modeling, analysis and simulation of optical wave propagation through the Earth's atmosphere is a challenging problem. This is mainly due to the presence of optical turbulence [1–3], a term that refers to the stochastic multi-scale variations in the index of refraction stemming from variations in density and temperature at similar scale. As waves propagate, these refractive index perturbations induce corresponding phase perturbations, which in turn, produces amplitude perturbations referred to as scintillation [4–6]. Compounding this problem further, the stochastic nature of these refractive index perturbations introduces uncertainty that often needs to be quantified.

In spite of the difficulties discussed above, there exists several approaches for simulating optical atmospheric propagation, each associated with a specific set of assumptions that tries to balance computational cost with fidelity. On one end of this spectrum are waveoptics simulations, where the atmosphere is modeled as a random media using a prescribed probability distribution. Discretized realizations are drawn from this distribution and used as inputs to a stochastic partial differential equation (PDE) that models optical propagation. The PDE typically used is the reduced wave equation, also known as the paraxial Helmholtz equation. This is derived from Maxwell's equations under the assumptions of small wavelength, i.e. in the optical regime [3], and a high degree of coherency in the propagating optical wave.Uncertainty is typically quantified through Monte-Carlo methods, where an ensemble of wave metrics are gathered and used to calculate statistics.

At the other end of the modeling spectrum are scaling laws, a term referring to a set of formulas derived from analysis (asymptotic or numerical) of the aforementioned stochastic PDEs used in the waveoptics approach. The objective in deriving these formulas is to map atmospheric statistics directly to statistics on the wave metrics without necessarily having to simulate the propagation directly, or to calculate the relevant statistics from the collected results of the ensemble of simulations. For example, the Rytov method gives a closed form representation for the first-order correction of a zeroth-order solution in the limit of small perturbations of the propagation medium [3, 7, 8]. This first-order wave correction takes the form of an integral over both the zeroth-order solution and the medium perturbations along the propagation path. In cases where the zeroth-order solutions can be expressed in close form, e.g. plane waves, these integrals can be evaluated exactly, or well-approximated, to form a mapping of atmospheric statistics to wave metrics [3, 7, 9, 10]. It should be noted, however, that these derivations are always dependent on assumptions that limit the regime over which the resulting scaling laws are valid. The most common assumption is that the size of the perturbations are small, as in the Rytov example above, but could also include assumptions that neglect interactions between the wave and propagation medium as in case of thermal blooming [11, 12], a well known nonlinear interaction. Nevertheless, these scaling law methods are commonly used to deliver first-order performance assessments of system design and deployment concepts [13–17].

This paper introduces a new approach to forming a scal-

ing law type approximation to the atmospheric propagation of optical beams based on a variational reformulation of the scalar stochastic paraxial Helmholtz equation commonly used in waveoptics simulations. Working with the Helmholtz equation in variational form allows approximations to be made through the use of suitably chosen trial functions, an approach that is commonly described as an extension of the Rayleigh-Ritz optimization procedure [18]. We begin by outlining a derivation of the paraxial Helmholtz equation and its reformulation as a variational problem. By introducing a trial solution in the form of parameterized Gaussian beam, we derive a set of stochastic ordinary differential equations (ODEs) that describe the evolution of these parameters as the beam propagates. The numerical results section shows how well this new scaling law performs in comparison to resolving the stochastic paraxial Helmholtz equation. To investigate the accuracy of this new method, we compare the average of an ensemble of realizations from both the variational formulation and a waveoptics approach. The two simulations are provided with equal initial conditions and atmospheric turbulence realizations. The results show that the variational scaling law performs reasonably well even under moderately high isotropic Kolmogorov turbulence conditions, greatly improving the computational cost of the calculation.

## MATHEMATICAL FORMULATION

A propagating optical wave is described by Maxwell's equations. Since the atmosphere has virtually no magnetic susceptibility, one can capture the traveling wave by only tracking the electric field of the light. After a few manipulations of Maxwell's equations, one arrives at a modified wave equation for the electric field:

$$\boldsymbol{\Delta}\mathbf{E}_\ell - \boldsymbol{\nabla}\left(\boldsymbol{\nabla}\cdot\mathbf{E}_\ell\right) - \frac{1}{c^2}\frac{\partial^2\mathbf{E}_\ell}{\partial t^2} = \mu_0\frac{\partial^2\mathbf{P}^\ell}{\partial t^2}, \tag{1}$$

where the subscript $\ell$ specifies the angular frequency ($\omega_\ell$) of the propagating wave, $c$ is the speed of causality, and $\mu_0$ represents the vacuum magnetic permeability. All interactions between the light and its medium are captured by the electric polarization term $\mathbf{P}^\ell = \mathbf{P}^\ell(\mathbf{E}_\ell)$. The relevant interactions for atmospheric propagation through turbulence includes only the real-valued background mean index of refraction of the air ($n_\ell^0$), a stochastic perturbation to this refractive index ($\delta n_{\text{turb}}$), and a constant linear loss caused by absorption and/or scattering in the atmosphere ($\alpha_{\text{loss}}^\ell$). Loss is usually treated as a negative gain in the medium, and is derived as an imaginary perturbation to the refractive index [19]. Mathematically, the electric polarization can be expressed as

$$\begin{aligned}
\mathbf{P}^\ell(\mathbf{E}_\ell) &\approx \mathbf{P}^\ell_{\text{background}}(\mathbf{E}_\ell) + \mathbf{P}^\ell_{\text{turb}}(\mathbf{E}_\ell) + \mathbf{P}^\ell_{\text{loss}}(\mathbf{E}_\ell)\\
\mathbf{P}^\ell_{\text{background}}(\mathbf{E}_\ell) &\approx \varepsilon_0\left(\left[\left(\mathbf{n}_\ell^0\right)^2 - \mathbf{1}\right]\mathbf{E}_\ell\right)\\
\mathbf{P}^\ell_{\text{turb}}(\mathbf{E}_\ell) &\approx 2\varepsilon_0\delta n_{\text{turb}}\mathbf{n}_\ell^0\mathbf{E}_\ell\\
\mathbf{P}^\ell_{\text{loss}}(\mathbf{E}_\ell) &\approx \frac{i\alpha_{\text{loss}}^\ell\varepsilon_0 c\mathbf{n}_\ell^0}{\omega_\ell}\mathbf{E}_\ell
\end{aligned}.$$

The vacuum electric permittivity is denoted as $\varepsilon_0$, and $\varepsilon_0\mu_0 = c^{-2}$. In this model, the light propagates in $+z$-direction, $\mathbf{E}_\ell = \mathbf{E}_\ell(\mathbf{r},t)$, $\mathbf{r} = (x,y,z)$, and $\mathbf{E}_\ell = \left[E_\ell^x\ E_\ell^y\ E_\ell^z\right]^{\mathrm{T}}$, where $[\cdot]^{\mathrm{T}}$ is the transpose operator.

It is assumed that the propagating light is highly coherent (from a laser source), and generally propagates in the $+z$-direction, making the $x,y$-directions transverse, which will be denoted with a $\perp$ symbol. Temporal coherence indicates that the light is near-monochromatic; other than the optical oscillation at the frequency $\omega_\ell$, the only other relevant timescales are that of the light travel time from the laser source to the target and that of the turbulence. This simulation assumes that the wavefront of the light can be propagated out to its endpoint (target) in a virtually static turbulence, since the turbulence changes over a much longer time period than the travel time. Spatial coherence indicates that the electric field can be well-approximated as a slowly varying envelope in the longitudinal direction that consistently oscillates in this direction at a frequency related to the wavenumber $k = n_\ell^0\omega_\ell/c$ of the field; this is known as the *paraxial approximation*. Moreover, omitting the small perturbation to the refractive index ($\delta n_{\text{turb}}$), the medium is mostly homogeneous, which means that Gauss's Law is applicable to this problem: $\boldsymbol{\nabla}\cdot\mathbf{E}_\ell \approx 0$ since there is no volume charge density. Additionally, it is assumed that the light is robustly linearly polarized in the $x$-direction, which means that $E_\ell^y$ and $E_\ell^z$ are negligibly small in comparison to $E_\ell^x$. Thus,

$$E_\ell^x(\mathbf{r},t) \approx \mathrm{Re}\left(A_\ell(\mathbf{r})\exp\left[ik^\ell z - i\omega_\ell t\right]\right),$$

where $\mathrm{Re}[\cdot]$ is the real-component-of operator, and $A_\ell(\mathbf{r})$ is the slowly varying envelop of the electric field. With this ansatz, and aforementioned approximations, one derives from the wave equation (1) the *paraxial stochastic Helmholtz equation*:

$$\frac{\partial A_\ell(\mathbf{r})}{\partial z} = \frac{i}{2k^\ell}\Delta_\perp A_\ell(\mathbf{r}) + ik_0^\ell\delta n_{\text{turb}}(\mathbf{r})A_\ell(\mathbf{r}) - \frac{\alpha_{\text{loss}}^\ell}{2}A_\ell(\mathbf{r}), \tag{2}$$

where $\Delta_\perp = \partial^2/\partial x^2 + \partial^2/\partial y^2$ is the transverse Laplacian operator, and $k_0^\ell = \omega_\ell/c$. Based on the previous argument that the light propagates to its endpoint nearly instantaneously in comparison to any temporal changes to the turbulence, the paraxial stochastic Helmholtz equation is time independent, solved with a particular turbulence realization. The statistics of the beam profile on target are found by solving this PDE multiple times, each with a new realization of the turbulence, which may be sampled from known statistics on $\delta n_{\text{turb}}(\mathbf{r})$.

This PDE can be nondimensionalized; first consider putting a "hat" [$\widehat{\cdot}$] over each parameter/variable in Eq. (2) in order to indicate that it has a dimension/unit. Next, make the following transformations: $\hat{x} = \widehat{l_0}x$, $\hat{y} = \widehat{l_0}y$, $\hat{z} = \widehat{L_0}z$, $\widehat{A_\ell} = \widehat{A_0}a$, $\widehat{\delta n_{\text{turb}}} = \sigma\delta n_{\text{turb}}$, $\xi = \widehat{l_0}^2\widehat{k_0^\ell}/\widehat{L_0}$, $\gamma = \widehat{l_0}\widehat{k_0^\ell}\sqrt{\sigma}$, and $\zeta = \widehat{l_0}^2\widehat{k_0^\ell}\widehat{\alpha_{\text{loss}}^\ell}$, where the unitless parameters/variables do not have "hats" over them. Moreover, for notational convenience, let $n \equiv n_\ell^0$. Note that $\sigma$ represents the strength of the atmospheric turbulence, and the stochastic perturbation to the refractive index ($\widehat{\delta n_{\text{turb}}}$) is actually unitless, but still uses a "hat" in order to distinguish it from its rescaling by $\sigma$. This yields

$$2in\xi\frac{\partial a}{\partial z}(\mathbf{r}) + \Delta_\perp a(\mathbf{r}) + 2n\gamma^2\delta n_{\text{turb}}(\mathbf{r})a(\mathbf{r}) + in\zeta a(\mathbf{r}) = 0. \tag{3}$$

Finally, $0 < \widehat{l_0} < \widehat{L_0}$ are length scales for the transverse and propagation dimensions that may be directly related to the inner and outer scales of the atmospheric turbulence (e.g., Kolmogorov turbulence [1, 2]), if one so chooses.

Typically the wavelength of the laser light is chosen so that it transmits well through the atmosphere with low loss. In fact, the loss parameter $\alpha_{\text{loss}}^\ell$ can be estimated using measured transmissions through the atmosphere [20]. Since the loss is a linear

effect that occurs over the distance traveled[1], it has negligible transverse effects on the traveling wave and its phase, unlike the turbulence. This means that it reasonable to treat the loss separately from the turbulence in the atmospheric propagation problem. This separation can be accomplished by breaking the governing PDE (3) into two equations as follows:

$$\frac{\partial a}{\partial z}(\mathbf{r}) = -\frac{\alpha}{2}a(\mathbf{r}) \tag{4}$$

$$\frac{\partial a}{\partial z}(\mathbf{r}) = \frac{i}{2n\xi}\Delta_\perp a(\mathbf{r}) + \frac{i\gamma^2}{\xi}\delta n_{\text{turb}}(\mathbf{r})a(\mathbf{r}), \tag{5}$$

where $\alpha = \zeta/\xi = \widehat{L_0\alpha^{\ell}_{\text{loss}}}$.

The loss Eq. (4) can be solved analytically with an initial condition: $a(x,y,0) = a_0\phi(x,y)$, where $a_0 \in \mathbb{C}$ and $\phi(x,y)$ is the initial, real-valued (without loss of generality) transverse profile of the propagating wavefront, yielding $a(\mathbf{r}) = a_0\phi(x,y)\exp(-\alpha z/2)$ or $|a(\mathbf{r})|^2 = |a_0|^2\phi^2(x,y)\exp(-\alpha z)$. On the other hand, the stochastic PDE for turbulence Eq. (5) ought to conserve the power in the wavefront as the light propagates; the beam may focus or spread out, change phase, or drift in the transverse direction from its original center position, but it will conserve power as it propagates in the longitudinal direction. Clearly, $|a_0|^2$, of the initial condition, is related to this power within the beam, especially if the beam profile is normalized such that $\int\int_{D_\perp}\phi^2(x,y)\,dxdy = 1$, where $D_\perp$ represents the transverse domain. The exponential factor $\exp(-\alpha z)$ attenuates that power as the light propagates. Therefore, since the solution to the lossless paraxial stochastic Helmholtz equation (5) reveals a conserved quantity, by attenuating that quantity according to the exponential factor, one captures the effect of atmospheric loss. The variational scaling law will focus on solving this paraxial stochastic Helmholtz equation (5) without loss.

### Variational Formulation

The theoretical framework for the variational scaling law was inspired by D. Anderson's works in [21–23], where the *variational approximation* was used to reduce the partial differential equation to the a lower-dimensional system. This variational approach relies on *Hamilton's principle*, and thus needs the governing dynamical system to have a conserved quantity, and since atmospheric loss has already been separated out, the propagating optical wave ought to conserve power.

The variational approach to atmospheric propagation involves recasting the propagation Eq. (5) in terms of the critical points of a functional

$$J(a,\nabla a) = \int_0^L\int_{-\infty}^{\infty}\int_{-\infty}^{\infty}\mathcal{L}_{\text{D}}(a,\nabla a)\;dxdydz, \tag{6}$$

where $\mathcal{L}_{\text{D}}$ is the *Lagrangian density*. These critical points (points where the derivative of the functional is zero) correspond to solutions of this PDE (5) through corresponding *Euler-Lagrange equations*:

$$\frac{\partial\mathcal{L}_D}{\partial a} - \sum_{i=1}^{3}\frac{\partial}{\partial r_i}\left(\frac{\partial\mathcal{L}_D}{\partial(\partial_{r_i}(a))}\right) = 0, \tag{7}$$

where $r_i \in \{x,y,z\}$ for $i = 1,2,3$, respectively. For the lossless paraxial stochastic Helmholtz equation:

$$\mathcal{L}_{\text{D}}(a,\nabla a) = -2n\xi\,\text{Im}\left(\bar{a}\frac{\partial a}{\partial z}\right) - \left|\nabla_\perp a\right|^2 + 2n\gamma^2\delta n_{\text{turb}}|a|^2. \tag{8}$$

[1]Note that the loss parameter $\alpha^{\ell}_{\text{loss}}$ has units of 1/m, indicating that its affect on the propagating wave grows with distance traveled.

Here, $[\cdot]$ denotes the conjugate operation, and $\text{Im}(\cdot)$ is the imaginary-component-of operator.

### General Gaussian Ansatz

The key to this method is the use of an ansatz, or trial solution, which defines the solution's dependence on a subset of the independent variables, and parameterizes the solution's dependence in the remaining independent variables. We illustrate the approach here with an ansatz where we assume the solution is well represented in the transverse direction (with respect to propagation), i.e. the variables $x$ and $y$, by a Gaussian profile

$$a(\mathbf{r}_\perp,\mathbf{p}(z)) = I(\mathbf{p}(z))e^{-\left(\Theta(\mathbf{r}_\perp,\mathbf{p}(z))+i\Phi(\mathbf{r}_\perp,\mathbf{p}(z))\right)}, \tag{9}$$

where

$$I(\mathbf{p}(z)) = \frac{C(z)\sqrt{W_x(z)W_y(z)}}{\sqrt{\pi}},$$

$$\Theta(\mathbf{r}_\perp,\mathbf{p}(z)) = \frac{1}{2}\left(W_x^2(z)\big(x-X(z)\big)^2 + W_y^2(z)\big(y-Y(z)\big)^2\right),$$

$$\Phi(\mathbf{r}_\perp,\mathbf{p}(z)) = P(z) + T_x(z)\big(x-X(z)\big) + T_y(z)\big(y-Y(z)\big) + F_x(z)\big(x-X(z)\big)^2 + F_y(z)\big(y-Y(z)\big)^2, \text{ and}$$

$$\mathbf{p}(z) = \big[C(z)\;W_x(z)\;W_y(z)\;T_x(z)\;T_y(z)\;X(z)\;Y(z)\;F_x(z)\;F_y(z)\;P(z)\big]^{\text{T}}.$$

Note, this ansatz is parameterized through a set of real-valued parameters (in $\mathbf{p}(z)$).

The terms of the Gaussian ansatz can be mapped to beam characteristics. For example, $I(\mathbf{p}(z))$ represents the peak of the beam amplitude, which depends on the parameters $W_x(z)$ and $W_y(z)$ – representing the beam width in the $x$ and $y$ directions, respectively, and the parameter $C(z)$, associated with the total beam power, i.e. $\int\int_{\mathbb{R}^2}|a(\mathbf{r}_\perp,\mathbf{p}(z))|^2\,dxdy = C^2(z)$. Likewise, $\Theta(\mathbf{r}_\perp,\mathbf{p}(z))$ controls the beam profile through the width parameters, and through the parameters $X(z)$, $Y(z)$, which represent the (transverse) beam profile center position. Finally, $\Phi(\mathbf{r}_\perp,\mathbf{p}(z))$ is the beam phase term, dependent on parameters for the piston $P(z)$, tip/tilt $T_x(z)$, $T_y(z)$ and focusing $F_x(z)$, $F_y(z)$. Finally, note that the ansatz is completely determined in transverse direction, so all evolution of the solution is now determined through the parameters of this trial solution. Adding more parameters would give the ansatz more degrees of freedom in which to evolve and capture more of the dynamics of the true solution. However, adding parameters arbitrarily could easily result in multiple parameters capturing the same evolution, while also severely complicating equations for this evolution discussed below. Rather, the parameters included in the ansatz should be, and, in this case, are, chosen carefully to reflect specific quantities and qualities of interest. They are also chosen according to knowledge of how the dynamics of the some parameters affect other parameters of a realistic propagating optical beam. For example, when parameters that account for tilt in the phase, i.e. $T_x(z)$ and $T_y(z)$, are included in the ansatz, then the corresponding parameters that capture shifts in the beam center, i.e. $X(z)$ and $Y(z)$, should also be included in the trial solution, since the phase tilt parameters alter the position of the beam center. This is a matter of completeness of the model.

Because the ansatz is completely determined in the transverse direction, the integrals over the transverse domain in relation (6) can be analytically evaluated, resulting in an averaged

Lagrangian $\mathcal{F}_{\mathrm{D}}$ for the dynamics captured by the parameterization

$$\mathcal{F}_{\mathrm{D}}\left(\mathbf{p}, \frac{d\mathbf{p}}{dz}\right) = \int_{-\infty}^{\infty}\int_{-\infty}^{\infty} \mathcal{L}_{\mathrm{D}}\left(\mathbf{r}_{\perp}, \mathbf{p}, \frac{d\mathbf{p}}{dz}\right) d\hat{x}d\hat{y}, \tag{10}$$

while also redefining the functional in Eq. (6) in terms of just the evolution of the parameters in $z$,

$$J\left(\mathbf{p}, \frac{d\mathbf{p}}{dz}\right) = \int_{0}^{L} \mathcal{F}_{\mathrm{D}}\left(\mathbf{p}, \frac{d\mathbf{p}}{dz}\right) dz. \tag{11}$$

Using the Gaussian ansatz in relations (8), (9), and (10) gives

$$\begin{aligned}\mathcal{F}_{\mathrm{D}}\left(\mathbf{p}, \frac{d\mathbf{p}}{dz}\right) &= 2n\xi C^2\left(\frac{dP}{dz} + \frac{\frac{dF_x}{dz}}{2W_x^2} + \frac{\frac{dF_y}{dz}}{2W_y^2}\right)\\ &- C^2\left(\frac{dX}{dz}T_x + \frac{dY}{dz}T_y\right) - \frac{C^2}{2}\left(W_x^2 + W_y^2\right)\\ &- C^2\left(T_x^2 + T_y^2\right) - 2C^2\left(\frac{F_x^2}{W_x^2} + \frac{F_y^2}{W_y^2}\right)\\ &+ 2n\gamma^2\left\langle \delta n_{\mathrm{turb}}, I^2 e^{-2\Theta}\right\rangle,\end{aligned} \tag{12}$$

where

$$\left\langle \cdot, * \right\rangle \equiv \int_{-\infty}^{\infty}\int_{-\infty}^{\infty} \cdot * \, dxdy$$

is an integration operation over the transverse domain, which can be interpreted as an innerproduct. As long as the laser field maintains a Gaussian profile, the evolution of the beam should be well-described by the dynamics captured in relations (11) and (12). Furthermore, these dynamics are also described through the corresponding set of Euler-Lagrange equations given by

$$\frac{\partial \mathcal{F}_{\mathrm{D}}}{\partial p_j} - \frac{d}{dz}\frac{\partial \mathcal{F}_{\mathrm{D}}}{\partial\left[\frac{dp_j}{dz}\right]} = 0 \tag{13}$$

for

$$p_j \in \left\{ \underbrace{C}_{j=1} \underbrace{W_x}_{j=2} \underbrace{W_y}_{j=3} \underbrace{T_x}_{j=4} \underbrace{T_y}_{j=5} \underbrace{X}_{j=6} \underbrace{Y}_{j=7} \underbrace{F_x}_{j=8} \underbrace{F_y}_{j=9} \underbrace{P}_{j=10} \right\}.$$

Note, turbulence is introduced through stochastic term $2n\gamma^2\left\langle \delta n_{\mathrm{turb}}, I^2 e^{-2\Theta}\right\rangle$, which can be interpreted as a projection of the stochastic index $\delta n_{\mathrm{turb}}$ onto the term $I^2 e^{-2\Theta}$, with $\gamma^2 = \left(\widehat{l_0 k_0^{\ell}}\right)^2 \sigma$ being a nondimensionalized strength of the stochastic index variations.

## Governing Equations

Applying the reduced Euler-Lagrange Eq. (13) to its corresponding reduced Lagrangian density Eq. (12), one derives

$$C(z) = C(0) \tag{14}$$

$$\frac{dW_x}{dz}(z) = \frac{2}{n\xi}F_x(z)W_x(z) \tag{15a}$$

$$\frac{dW_y}{dz}(z) = \frac{2}{n\xi}F_y(z)W_y(z) \tag{15b}$$

$$\frac{dT_x}{dz}(z) = -n\gamma^2\left\langle \delta n_{\mathrm{turb}}(\mathbf{r}), M_{T_x}(\mathbf{r})\right\rangle \tag{15c}$$

$$\frac{dT_y}{dz}(z) = -n\gamma^2\left\langle \delta n_{\mathrm{turb}}(\mathbf{r}), M_{T_y}(\mathbf{r})\right\rangle \tag{15d}$$

$$\frac{dX}{dz}(z) = -2T_x(z) \tag{15e}$$

$$\frac{dY}{dz}(z) = -2T_y(z) \tag{15f}$$

$$\frac{dF_x}{dz}(z) = -\frac{W_x^4(z)}{2n\xi} + \frac{2F_x^2(z)}{n\xi} + \frac{\gamma^2}{\xi}\left\langle \delta n_{\mathrm{turb}}(\mathbf{r}), M_{F_x}(\mathbf{r})\right\rangle \tag{15g}$$

$$\frac{dF_y}{dz}(z) = -\frac{W_y^4(z)}{2n\xi} + \frac{2F_y^2(z)}{n\xi} + \frac{\gamma^2}{\xi}\left\langle \delta n_{\mathrm{turb}}(\mathbf{r}), M_{F_y}(\mathbf{r})\right\rangle \tag{15h}$$

$$\frac{dP}{dz}(z) = \frac{\left(W_x^2(z) + W_y^2(z)\right)}{2n\xi} - \frac{\gamma^2}{\xi}\left\langle \delta n_{\mathrm{turb}}(\mathbf{r}), M_P(\mathbf{r})\right\rangle \tag{15i}$$

where

$$M_{T_x}(\mathbf{r}) := \frac{2}{C^2(z)}\frac{\partial\left|a\left(\mathbf{r}_{\perp}, \mathbf{p}(z)\right)\right|^2}{\partial X} = 4W_x^2\left(x - X\right)\frac{|a|^2}{C^2}$$

$$M_{T_y}(\mathbf{r}) := \frac{2}{C^2(z)}\frac{\partial\left|a\left(\mathbf{r}_{\perp}, \mathbf{p}(z)\right)\right|^2}{\partial Y} = 4W_y^2\left(y - Y\right)\frac{|a|^2}{C^2}$$

$$M_{F_x}(\mathbf{r}) := \frac{W_x^3(z)}{C^2(z)}\frac{\partial\left|a\left(\mathbf{r}_{\perp}, \mathbf{p}(z)\right)\right|^2}{\partial W_x} = W_x^2\left[1 - 2W_x^2\left(x - X\right)^2\right]\frac{|a|^2}{C^2}$$

$$M_{F_y}(\mathbf{r}) := \frac{W_y^3(z)}{C^2(z)}\frac{\partial\left|a\left(\mathbf{r}_{\perp}, \mathbf{p}(z)\right)\right|^2}{\partial W_y} = W_y^2\left[1 - 2W_y^2\left(y - Y\right)^2\right]\frac{|a|^2}{C^2}$$

$$\begin{aligned}M_P(\mathbf{r}) &:= \frac{W_x(z)}{2C^2(z)}\frac{\partial\left|a\left(\mathbf{r}_{\perp}, \mathbf{p}(z)\right)\right|^2}{\partial W_x} + \frac{W_y(z)}{2C^2(z)}\frac{\partial\left|a\left(\mathbf{r}_{\perp}, \mathbf{p}(z)\right)\right|^2}{\partial W_y} +\\ &\frac{1}{2C(z)}\frac{\partial\left|a\left(\mathbf{r}_{\perp}, \mathbf{p}(z)\right)\right|^2}{\partial C}\\ &= \left[2 - W_x^2\left(x - X\right)^2 - W_y^2\left(y - Y\right)^2\right]\frac{|a|^2}{C^2}\end{aligned}$$

Finally, the atmospheric loss due to absorption/scattering can be reintroduced by replacing the conservation of the amplitude magnitude relation (14) with

$$C(z) = C(0)e^{-\frac{\alpha z}{2}}, \tag{16}$$

in accordance with the arguments concerning the loss relation (4).

Therefore, the variational scaling law consists of 9 coupled stochastic ODEs (15a-i) that can either exclude atmospheric loss, using relation (14), or include atmospheric loss, using relation (16). Compare the fact that a numerical solver for the paraxial stochastic Helmholtz Eq. (3) requires that one tracks a large number of discrete points (a $10^3$ by $10^3$ grid gives $10^6$

points), in the transverse domain along the longitudinal propagation axis, whereas this new system requires that one to track 9 parameters over the same distance. However, the variational scaling law still integrates over the transverse domain at every discrete longitudinal step.

### Gaussian Markov Approximations

A typical assumption for the turbulence-induced perturbation to the refractive index is that it has a Gaussian probability distribution with a zero mean (or expected value) and a known standard deviation $\sigma_{\delta n}$:

$$\mathbb{E}\left[\widehat{\delta n}(\hat{\mathbf{r}})\right] = 0, \qquad \mathbb{E}[\delta n(\mathbf{r})] = 0,$$
$$\sqrt{\mathbb{V}\left[\widehat{\delta n}(\hat{\mathbf{r}})\right]} = \sigma_{\delta n}, \qquad \sqrt{\mathbb{V}[\delta n(\mathbf{r})]} = 1,$$

where $\widehat{\delta n} = \sigma \delta n$, and the subscript "turb" has been dropped for notational convenience. This choice offers another convenient property for the correlation between the perturbations of the refractive index at any two spatial positions:

$$\begin{aligned}\operatorname{cor}(\delta n(\mathbf{r}_1), \delta n(\mathbf{r}_2)) &:= \frac{\mathbb{E}\left[\prod_{i=1}^{2} (\delta n(\mathbf{r}_i) - \mathbb{E}[\delta n(\mathbf{r}_i)])\right]}{\prod_{i=1}^{2} \sqrt{\mathbb{V}[\delta n(\mathbf{r}_i)]}} \\ &= \mathbb{E}[\delta n(\mathbf{r}_1)\delta n(\mathbf{r}_2)]\,.\end{aligned}$$

Furthermore, it is common to assume that this perturbation to the index of refraction is delta-correlated in the propagation (longitudinal) direction of the light (referred to as the Markov Assumption [3]):

$$\operatorname{cor}(\delta n(\mathbf{r}_1), \delta n(\mathbf{r}_2)) = \operatorname{cor}(\delta n(x_1, y_1), \delta n(x_2, y_2))\, \delta_{\mathrm{D}}(z_1 - z_2),$$

where $\delta_{\mathrm{D}}$ represents the Dirac delta function.

As indicated in the governing ODEs (15a-i), the evolution of the Gaussian beam contains continuous perturbations due to the overlap of the stochastic of refraction variations with, what will be called, Gaussian parameter modes ($M_j$): $\kappa_{\delta n, M} := \langle \delta n, M \rangle$. Since the modes ($M_j$) are deterministic, the mean of this overlap is

$$\mathbb{E}\left[\kappa_{\delta n, M}\right] = \langle \mathbb{E}[\delta n]\,, M \rangle = 0,$$

In addition, the covariance between any two perturbations is given by

$$\begin{aligned}&\operatorname{cov}\left(\kappa_{\delta n, M_1}(\mathbf{r}_1), \kappa_{\delta n, M_2}(\mathbf{r}_2)\right) = \\ &\quad \delta_{\mathrm{D}}(z_1 - z_2) \iiint_{-\infty}^{\infty} \operatorname{cor}(\delta n(x_1, y_1), \delta n(x_2, y_2)) \cdot \\ &\quad M_1(x_1, y_1, z_1) M_2(x_2, y_2, z_1)\, dx_1 dy_1 dx_2 dy_2\end{aligned} \tag{17}$$

Note that $M_1 \equiv M_2$ does not imply that $\mathbf{r}_1 \equiv \mathbf{r}_2$, and vice-versa.

Given these properties on the refractive index perturbation, the stochastic terms in (15a-i) can be replaced by simple delta correlated Gaussian processes in the variable $z$

$$\mathcal{T}_x(z) = \langle \delta n_{\mathrm{turb}}(\mathbf{r}), M_{T_x}(\mathbf{r}) \rangle \tag{18}$$
$$\mathcal{T}_y(z) = \left\langle \delta n_{\mathrm{turb}}(\mathbf{r}), M_{T_y}(\mathbf{r}) \right\rangle \tag{19}$$
$$\mathcal{F}_x(z) = \langle \delta n_{\mathrm{turb}}(\mathbf{r}), M_{F_x}(\mathbf{r}) \rangle \tag{20}$$
$$\mathcal{F}_y(z) = \left\langle \delta n_{\mathrm{turb}}(\mathbf{r}), M_{F_y}(\mathbf{r}) \right\rangle \tag{21}$$
$$\mathcal{P}(z) = \langle \delta n_{\mathrm{turb}}(\mathbf{r}), M_P(\mathbf{r}) \rangle \tag{22}$$

with correlation matrix elements given by relation (17).

This leads to a reduced version of the variational scaling law that is less computationally expensive when the stochastic terms in (15a-i) are replaced by the five Gaussian processes defined above. This approximation of the stochastic terms eliminates the need to generate a set of perturbations to the index of refraction, $\delta n_{\mathrm{turb}}$, and the subsequent integration over the transverse plane. In this simplified model, we instead draw realizations of each of the five Gaussian processes which is computationally cheap compared to the generation of $\delta n_{\mathrm{turb}}$.

## NUMERICAL MODEL RESULTS

To illustrate that the variational scaling law (VSL) well-approximates the solution to the paraxial stochastic Helmholtz equation, the statistics, especially the average, of an ensemble of the beam propagation realizations from the solution to the Helmholtz equation is compared to the average result from the VSL approach. Note that the ensemble statistics for the VSL converge with fewer realizations compared to the waveoptics approach. However, in the results presented below, the ensemble statistics are computed for 400 realizations of both models. For these comparisons, the VSL and the paraxial Helmholtz equation are supplied with the same initial conditions, and the perturbation to the index of refraction are randomly sampled using the same statistical characteristics. The realizations of the index of refraction at any given discrete longitudinal point are generated using the *circulant embedding* method outlined in [24].

The stochastic paraxial Helmholtz equation (the waveoptics approach) is solved via a Strang-splitting (split-step) scheme in which the stochastic term is treated separately from the diffusive term. A Strang-splitting scheme is a standard numerical method for solving partial differential equations, including the paraxial Helmholtz equation [25, 26]. In this model, the transverse plane is equipped with periodic boundary conditions; however, the transverse domain is always chosen large enough that the beam does not substantially encounter these periodic boundaries. The diffusive term is treated with the fast Fourier transform (FFT) algorithm, and the stochastic term is viewed as a phase contribution for each particular realization of the refractive index ($\delta n_{\mathrm{turb}}$). For simplicity, the governing set of stochastic ODEs corresponding to the VSL is solved via the backwards Euler implicit method.

### Atmospheric Turbulence Statistics and Properties

Optical turbulence is typically represented through the Kolmogorov model [3] in which the stochastic variations of the index of refraction are described by the structure function:

$$\begin{aligned}&\mathbb{E}\left[\left(\delta n(\boldsymbol{r}_{1,\perp}) - \delta n(\boldsymbol{r}_{2,\perp})\right)^2\right] = 2\left(1 - \operatorname{cor}(\delta n(\boldsymbol{r}_1), n(\boldsymbol{r}_2))\right) \\ &= \frac{\widehat{C_n}^2 \widehat{l_0}^{\frac{2}{3}}}{\sigma_n^2} \begin{cases} \left|\boldsymbol{r}_{1,\perp} - \boldsymbol{r}_{2,\perp}\right|^2, & \text{for } 0 < \left|\boldsymbol{r}_{1,\perp} - \boldsymbol{r}_{2,\perp}\right| \le 1 \\ \left|\boldsymbol{r}_{1,\perp} - \boldsymbol{r}_{2,\perp}\right|^{\frac{2}{3}}, & \text{for } 1 < \left|\boldsymbol{r}_{1,\perp} - \boldsymbol{r}_{2,\perp}\right| \le \frac{1}{\epsilon} \end{cases},\end{aligned}$$

where $\epsilon = \widehat{l_0}/\widehat{L_0}$, and $\widehat{l_0}$ and $\widehat{L_0}$ are the characteristic length scales used to nondimensionalize the transverse and propagation directions, respectively. Thus, the correlation function is represented as

$$\begin{aligned}&\operatorname{cor}(\delta n_1, \delta n_2) = 1 - \\ &\frac{\widehat{C_n}^2 \widehat{l_0}^{\frac{2}{3}}}{2\sigma_n^2} \begin{cases} \left|\boldsymbol{r}_{1,\perp} - \boldsymbol{r}_{2,\perp}\right|^2, & \text{for } 0 < \left|\boldsymbol{r}_{1,\perp} - \boldsymbol{r}_{2,\perp}\right| \le 1 \\ \left|\boldsymbol{r}_{1,\perp} - \boldsymbol{r}_{2,\perp}\right|^{\frac{2}{3}}, & \text{for } 1 < \left|\boldsymbol{r}_{1,\perp} - \boldsymbol{r}_{2,\perp}\right| \le \frac{1}{\epsilon} \end{cases}.\end{aligned}$$

If we assume that $|\mathrm{cor}(\delta n_1, \delta n_2)| \approx 0$ for $|\boldsymbol{r}_{1,\perp} - \boldsymbol{r}_{2,\perp}| \approx 1/\epsilon$, then the variance of the index of refraction can be approximated as

$$\sigma_n^2 \approx \frac{\widehat{C_n^2}\widehat{L_0}^{2/3}}{2} \text{ and}$$
$$\mathrm{cor}(n_1, n_2) = 1 - \begin{cases} |\boldsymbol{r}_1 - \boldsymbol{r}_2|^2, & \text{for } 0 < |\boldsymbol{r}_1 - \boldsymbol{r}_2| \le 1 \\ |\boldsymbol{r}_1 - \boldsymbol{r}_2|^{2/3}, & \text{for } 1 \le |\boldsymbol{r}_1 - \boldsymbol{r}_2| \le 1/\epsilon \end{cases}.$$

Note that $\sigma_n \equiv \sigma$ from the nondimensional parameters.

In the numerical implementations for both the VSL and the waveoptics model, the atmospheric turbulence is being represented by a layered-atmosphere model [27, 28]. In this approach, we begin with a continuous, constant index structure profile, $\widehat{C_n^2}(\hat{z}) = C_0$, and use this to compute an *effective index structure constant*, $\widehat{C_{n,i}^2}$ for each numerical propagation step. The effective index structure constant is selected such that many of the low-order moments of the continuous model are equal to the layered model:

$$\int_0^{\hat{L}} \widehat{C_n^2}(\hat{z'})(\hat{z'})^m d\hat{z'} = \sum_{i=1}^{N_z} \widehat{C_{n,i}^2}\hat{z}_i^m \Delta\hat{z}, \quad 0 \le m \le 7 \qquad \textbf{(23)}$$

where $N_z$ is the number of propagation steps in the $z$-direction, $\hat{L}$ is the propagation distance, and $\Delta\hat{z} = \hat{L}/N_z$ is the $z$-step size. To measure the strength of the turbulence, the Fried parameter, $\hat{r}_0(\hat{z})$, and the Rytov variance, $\sigma_R^2(\hat{z})$, is calculated with the effective index structure constant [28]. Note that, when $\sigma_R^2(\hat{z}) < 0.25$, the model conditions represent weak turbulence, and when $\sigma_R^2(\hat{z}) \gg 0.25$, the model conditions represent strong turbulence. For the numerical results in the following, we use three turbulence strengths to assess the VSL, $\widehat{C_n^2}(\hat{z}) = 1 \cdot 10^{-16}$, $4 \cdot 10^{-16}$, and $9 \cdot 10^{-16}\ m^{-2/3}$. The corresponding Fried parameters and Rytov variances, for $\hat{z} = 6000$ m, are presented in Table 1.

**Table 1.** The Fried parameters and Rytov variances at 6000 m.

| $\widehat{C_n^2}$ | $\hat{r}_0$ | $\sigma_R^2$ | turbulence strength |
|---|---|---|---|
| $1 \cdot 10^{-16}$ | 0.18 | 0.046 | weak |
| $4 \cdot 10^{-16}$ | 0.10 | 0.18 | medium |
| $9 \cdot 10^{-16}$ | 0.06 | 0.41 | strong |

These turbulence statistical properties paired with the effective index structure constant are used in the numerical results presented hereafter for both the VSL and the waveoptics model.

### Model Parameters

For the numerical comparison the VSL and the waveoptics model (scalar paraxial stochastic Helmholtz equation) are initialized as follows. First, the dimensional constants and characteristic scales are defined, and then the nondimensional counterparts are calculated. When computing the model parameters that depend on the index structure constant, $\widehat{C_n^2}$, we instead utilize the set of effective index structure constants, $\{\widehat{C_{n,i}^2}\}_{i=1,\dots,N_Z}$, to compute effective model parameters. Particularly, a set of effective index structure variance parameters, $\sigma_i^2$, is computed using

$$\sigma_{n,i}^2 = \frac{\widehat{C_{n,i}^2}\widehat{L_0}^{2/3}}{2}, \quad i = 1, \dots N. \qquad \textbf{(24)}$$

The effective variance parameter is then used to compute the effective scaled turbulence strength, $\gamma_i^2 = (\widehat{l_0}\widehat{k_0})^2\sigma_{n,i}$, to be used in the numerical simulations for both models. The values of the physical constants used for the proceeding numerical results are given in Table 2, and their corresponding scaled quantities are presented in Table 3. The effective parameters, $\widehat{C_{ni}^2}$, $\gamma_i$, and $\sigma_i^2$ are no longer constant over the propagation distance, so their values are not reported in Table 2 and Table 3. Since loss is not being considered: $\zeta = 0$.

**Table 2.** The values of the physical constants and characteristic scales that describe the propagating laser field.

| physical quantity | symbol | value |
|---|---|---|
| wavelength | $\widehat{\lambda}$ | $10^{-6}$ m$^{-1}$ |
| inner-scale | $\widehat{l_0}$ | $10^{-3}$ m |
| outer-scale | $\widehat{L_0}$ | $10^{2}$ m |
| aperture diameter | $\widehat{D}$ | $2 \cdot 10^{-2}$ m |
| propagation distance | $\widehat{L_z}$ | 6000 m |
| background index | $\hat{n}$ | $1 + 10^{-6}$ |
| transverse length $x$ | $\widehat{L_x}$ | 1.25 m |
| transverse length $y$ | $\widehat{L_y}$ | 1.25 m |

**Table 3.** A listing of some scaled quantities and their corresponding values based on the given parameters of Table 2.

| computational quantity | symbol | value |
|---|---|---|
| transverse length $x$ | $L_x = \widehat{L_x}/\widehat{l_0}$ | 625 |
| transverse length $y$ | $L_y = \widehat{L_y}/\widehat{l_0}$ | 625 |
| propagation distance | $L_z = \widehat{L_z}/\widehat{L_0}$ | 60 |
| scaled aperture | $D = \widehat{D}/\widehat{l_0}$ | 20 |
| wavenumber strength | $\xi = \widehat{l_0}^2\widehat{k_0^\ell}/\widehat{L_0}$ | 0.0623 |
| loss strength | $\zeta = \widehat{l_0}^2\widehat{k_0^\ell}\widehat{\alpha_{\text{loss}}^\ell}$ | 0 |

### Initial Conditions

The initial condition for both the VSL and the waveoptics model will be given by the Gaussian ansatz (9), using the ten parameters that describe the Gaussian. We will consider two initial conditions, both of which are inspired by the deterministic Gaussian beam profile as described in the 2001 paper by Andrews et al. [9]. Specifically, for the turbulence strength analysis, we use the following initial parameters for a symmetrical focusing

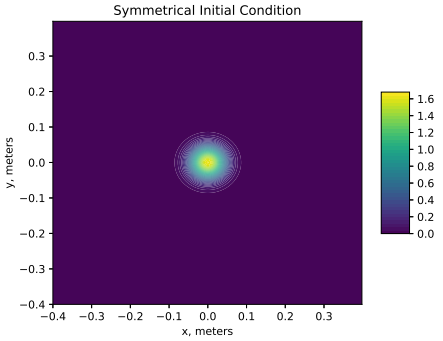


**Fig. 1.** The symmetrical initial condition irradiance.

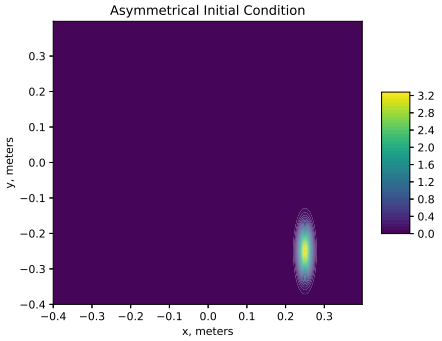


**Fig. 2.** The asymmetrical initial condition irradiance.

Gaussian beam, centered on the origin, without any tip/tilt:

$$\begin{aligned} C(0) &= 100 = C \\ W_x(0) = W_y(0) &= \frac{w_0\sqrt{n_0\alpha}}{\sqrt{w_0^4 + (0-z_w)^2}} \\ T_x(0) = T_y(0) &= 0 \\ X(0) = Y(0) &= 0 \\ F_x(0) = F_y(0) &= \frac{-0.5 n_0 \alpha (0-z_w)}{w_0^4 + (0-z_w)^2} \\ P(0) &= -\arctan\left(\frac{z_w}{w_0^2}\right) \end{aligned} \quad , \tag{25}$$

where $z_w$ is a specified scaled location and $w_0$ is the initial beam waist size. The location is prescribed to be $z_w = 50$, and the initial beam waist size is taken to be one quarter the diameter of the computational domain diameter: $w_0 = D/4 = 5$. The second initial condition is a modification of the first one to incorporate asymmetry and tip/tilt into the model. The initial parameters that have changed from the first initial condition, Eq. (25), to the second initial condition are: $W_x(0) = 4W_y(0)$, $T_x(0) = 0.25$, $T_y(0) = -0.5$, $X(0) = 250$, and $Y(0) = -250$. In vacuum propagation, the second initial condition represents a beam whose center travels from the bottom right to the top middle in the transverse plane.

Note that the beam width parameters in the VSL are proportional to the inverse of the physical width of the beam. With this initial condition, any tilt in the system is strictly introduced through the interaction of the beam with the turbulent atmosphere. In vacuum, i.e. $\delta n_{\text{turb}} = 0$, this initial condition choice allows us to know apriori the beam waist size and location. This is helpful for the case of weak atmospheric turbulence because we can expect that the beam waist size and location will be a perturbation away from the prescribed location in the initial condition. The initial irradiance for the symmetrical initial condition is in Fig. 1 and the asymmetrical initial condition is in Fig. 2. Note that the figures are presented in dimensional units.

From the derivation of the models, it is expected that the total beam power is conserved throughout the propagation distance for both VSL and waveoptics. Thus, it is important to ensure the selected numerical methods for both models still conserve the total beam power. This can be easily checked by simply computing

$$C(z) \approx \left(\int_{-L}^{L}\int_{-L}^{L} |a|^2 dxdy\right)^{1/2}$$

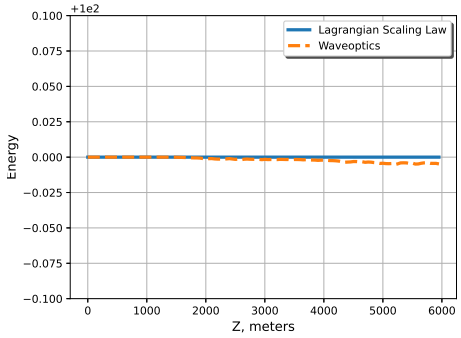


**Fig. 3.** The beam power is conserved for both VSL and waveoptics, $C(\widehat{Z}) \approx C(0) = 100$ for all $\widehat{Z}$. Note that the vertical axis is scaled from $[99.9, 100.1]$.

at each propagation step and we expect this to remain equal to the initial power of the beam. Fig. 3 shows the conservation of beam power over the propagation length for both models. The waveoptics approach shows a slight decrease in power, but it is equivalent a 0.0048% difference from the initial power of 100.

### Symmetric Initial Condition Comparison to Waveoptics

To assess the accuracy of the VSL in comparison to the waveoptics approach, an ensemble of 400 independent runs/realizations is conducted, and the average irradiance from both models are compared using the turbulence strengths in Table 1 for the symmetrical initial condition. In this section and the next, the figures show results for the medium turbulence strength, and note that the colorbar scale may differ from figure to figure.

To compare the difference in the value of the average peak irradiance from the two models we look at one-dimensional slices through the irradiance profile in both the $x$- and $y$-directions. Recall, the irradiance is found as the magnitude squared of the electric field. The errors are computed with the discrete 2-norm as relative errors such that the waveoptics solution is considered to be trusted. For notational convenience, let $I_p^L(x,y)$ be the peak irradiance from the VSL solution and $I_p^H(x,y)$ be the peak irradiance from the waveoptics solution. If we let $I(x,y)$ represent one of the above irradiances, then an $x$-slice through the irradiance is defined to be $I_x(y) = I(0,y)$ and a $y$-slice is defined to be $I_y(x) = I(x,0)$. The average peak irradiance profile, $I_y(x)$, for medium turbulence, is shown in Fig. 4. The relative error between the irradiance profiles is reported in Table 4.

Another measure for the accuracy is given by tracking the

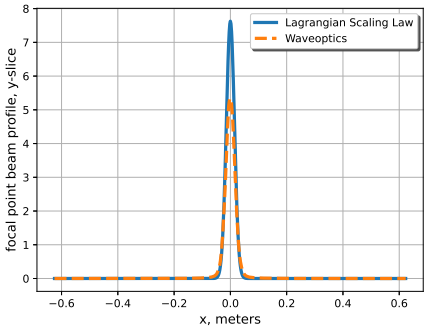


**Fig. 4.** A comparison of a slice through the average irradiance along the line $x = 0$ at $\widehat{z} = 5000$ m ($\sigma_R^2 = 0.18$).

value of the peak irradiance. For the VSL solution, this is simply given by the irradiance at the center of the Gaussian, which is at the mesh coordinates nearest to the $X = X(z)$ and $Y = Y(z)$ variables. In the case of waveoptics, the location of the center irradiance is approximated numerically from the average of the ensemble. The center irradiance of the VSL solution will be denoted by $I^L_{\text{center}}(z)$, and the average center irradiance of the waveoptics solution will be denoted by $I^H_{\text{center}}(z)$. The center irradiance is recorded for each propagation step, and again the relative error between the two models is measured in the 2-norm. The relative error for the peak irradiance along the propagation path is shown in Table 5, and illustrated in Fig. 5.

Another metric of comparison is found in the width of the beam. This width evolves as the light propagates, and the absolute peak irradiance over the propagation distance ought to correspond to the minimum beam width (the focal point). As a standard convention, the overall beam width for a given 1D slice through the Gaussian irradiance is bounded by the locations were the irradiance diminishes by a factor of $1/e^2$ from its peak. Again, only two slices centered on the $x$- and $y$-axes will be used for this calculation, producing a width value for each slice. Over the propagation distance, the relative error, measured in 2-norm, of the beam width, calculated separately for the $x$- and $y$-slices through the irradiance profile, are given in Table 6.

The evolution of this beam width for the $y$-slice is depicted in Fig. 6 when $\sigma_R^2 = 0.18$. Lastly, we consider the relative error in

**Table 4.** The relative error of the average the irradiance $x$- and $y$-axis profiles.

| $\sigma_R^2$ | $x$-slice error | $y$-slice error |
|---|---|---|
| 0.046 | $2.30 \cdot 10^{-1}$ | $2.41 \cdot 10^{-1}$ |
| 0.18 | $3.62 \cdot 10^{-1}$ | $3.41 \cdot 10^{-1}$ |
| 0.41 | $7.52 \cdot 10^{-1}$ | $8.13 \cdot 10^{-1}$ |

**Table 5.** The relative error of the average center irradiance.

| $\sigma_R^2$ | center irradiance error |
|---|---|
| 0.046 | $9.6 \cdot 10^{-2}$ |
| 0.18 | $3.68 \cdot 10^{-1}$ |
| 0.41 | $6.73 \cdot 10^{-1}$ |

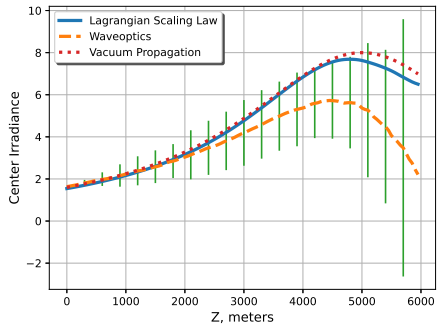


**Fig. 5.** A comparison of the average center irradiance as a function of propagation distance ($\sigma_R^2 = 0.18$).

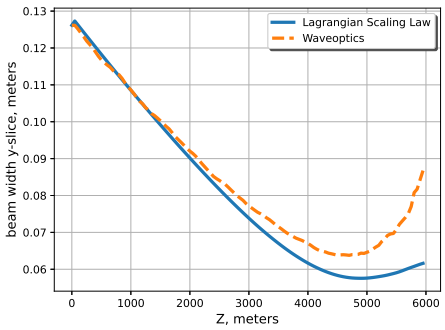


**Fig. 6.** A comparison of the beam width as calculated from the centered $y$-slice through the irradiance profile ($\sigma_R^2 = 0.18$).

focal point/beam waist location in propagation, $\widehat{z_w}$. In vacuum propagation, the beam waist location of the symmetric focusing Gaussian beam initial condition is at $\widehat{z_w} = 5000$ m. In the presence of turbulence the location of the beam waist fluctuates and, on-average, it occurs slightly before the vacuum propagation beam waist location. The relative error in the beam waist location in propagation is given in Table 7.

As shown by this example, the VSL well-approximates the solution to the waveoptics approach in the presence of weak turbulence, $\sigma_R^2 < 0.25$. The approximation the VSL provides

**Table 6.** The relative error of the beam width, calculated for $x$- and $y$-slices through the irradiance profile.

| $\sigma_R^2$ | $x$ beam width error | $y$ beam width error |
|---|---|---|
| 0.046 | $2.3 \cdot 10^{-2}$ | $2.3 \cdot 10^{-2}$ |
| 0.18 | $7.46 \cdot 10^{-2}$ | $7.16 \cdot 10^{-2}$ |
| 0.41 | $1.83 \cdot 10^{-1}$ | $1.72 \cdot 10^{-1}$ |

**Table 7.** The relative error of the propagation location of the focal point or beam waist for the symmetric initial condition.

| $\sigma_R^2$ | relative error in $\widehat{z_w}$ |
|---|---|
| 0.046 | $3.12 \cdot 10^{-2}$ |
| 0.18 | $8.11 \cdot 10^{-2}$ |
| 0.41 | $9.35 \cdot 10^{-2}$ |

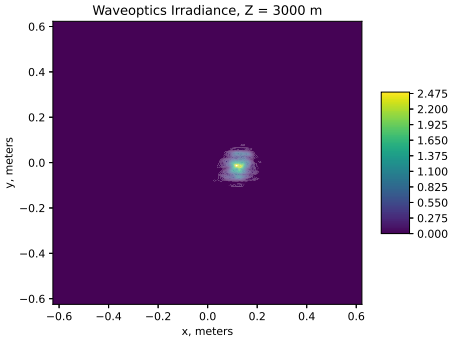


**(a)** Waveoptics Irradiance, $\widehat{z} = 3000$ m

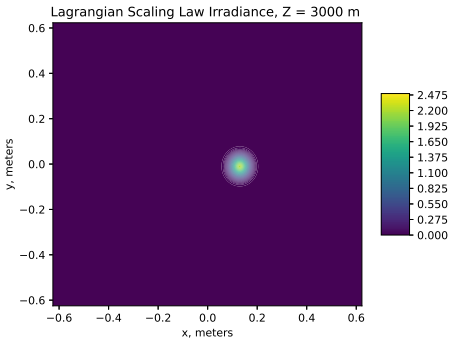


**(b)** LSL Irradiance, $\widehat{z} = 3000$ m.

**Fig. 7.** A comparison irradiance at $\widehat{z} = 3000$ m computed with *one* ensemble run of each model for $\sigma_R^2(3000) = 0.108$.

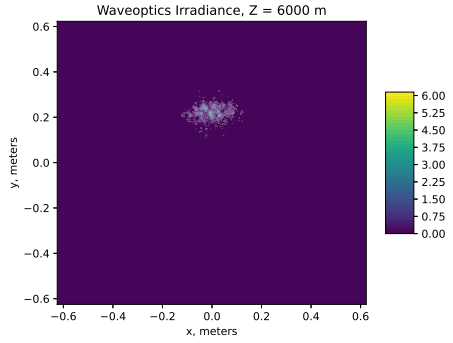


**(a)** Waveoptics Irradiance, $\widehat{z} = 6000$ m

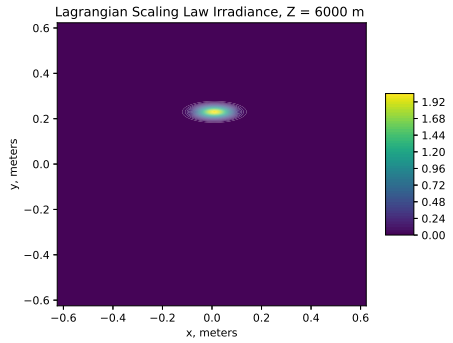


**(b)** LSL Irradiance, $\widehat{z} = 6000$ m.

**Fig. 8.** A comparison irradiance at $\widehat{z} = 6000$ m computed with *one* ensemble run of each model for $\sigma_R^2(6000) = 0.18$.

deteriorates in the strong turbulence regime, which is expected since the VSL was derived under the assumption of weak turbulence. However, in presence of strong turbulence, the VSL still well-approximates the beam width and location of the focal point, despite the poor approximation in the average center irradiance value.

### Asymmetrical Initial Condition Comparison to Waveoptics

In this section, we compare the VSL to waveoptics simulations with an initial condition of nonzero tip/tilt. The asymmetrical initial irradiance for this initial condition is shown in Fig. 2. From vacuum propagation with the asymmetric initial condition, we expect the beam center to move from the bottom right corner to the top middle of the transverse plane.

The irradiance for each model at propagation distances $\widehat{Z} = 3000$ m and $\widehat{Z} = 6000$ m are shown in Figs. 7 and 8, respectively. Qualitatively, we can see that the waveoptics irradiance is roughly the equal to the VSL irradiance.

Particularly, the $y$-coordinate of the beam center increases from $-0.25$ to approximately 0.2 and the $x$-coordinate of the beam decreases from 0.25 to approximately 0. This is confirmed by comparing the average value of the beam's center coordinates for both models over the ensemble average, see Fig. 9. The average value of the center coordinates for the VSL is computed as the ensemble average of the beam parameters $X(z)$ and $Y(z)$, and for the waveoptics simulations the center coordinates are approximated from the average irradiance. The relative error, computed over the propagation distance, is in the average beam center coordinates is shown in Table 8.

Lastly, we compare the value of the average center irradiance for the asymmetric initial condition. Fig. 10 shows the center irradiance value over the propagation distance for the VSL, the waveoptics model, and vacuum propagation, and the corresponding relative error can be found in Table 8. For the considered levels of turbulence, we feel that these errors between the VSL and the waveoptics model are quite reasonable; though the final judgement of *acceptable error* is left to the subject matter expert and the particulars of the given simulations.

## CONCLUSIONS

The variational scaling law offers a fast, reliable method for calculating a first-order approximation to laser light atmospheric propagation. This may have many important directed energy beam control applications in the areas of scene generation, target detection, tracking, aimpoint maintenance, adaptive optics/atmospheric correction, et cetera. At this point, one run of the VSL currently achieves $\sim$ 2x computation speed-up compared to one run of the waveoptics model. Further computational speed-up can be achieved by leveraging the simplifications outlined in the Gaussian Markov approximation subsection, and this will be explored in future work. Most notably, the VSL exhibits $>$ 100x memory reduction when compared to the waveoptics model. In the VSL, the ten Gaussian parameters must be tracked over the course of propagation, on the other hand, the waveoptics model requires tracking the full transverse-field over the course of propagation. The memory reduction achieved by the VSL is dependent on the discretization parameters used in the waveoptics model. In the presence of weak atmospheric turbulence, the VSL well-approximates the evolution of a Gaussian beam computed via the waveoptics model. There are however some limitations to this VSL

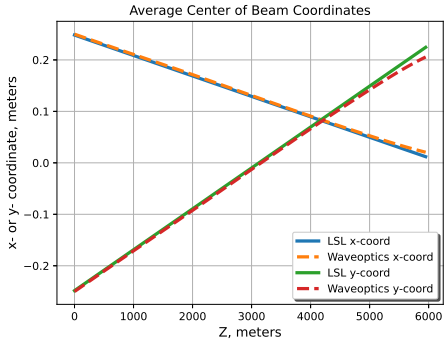


**Fig. 9.** The ensemble average of the center coordinates of the beam for the asymmetrical initial condition when $\sigma_R^2 = 0.18$.

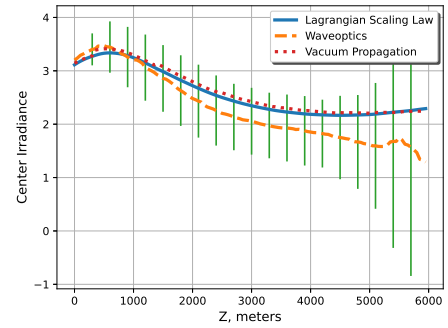


**Fig. 10.** The ensemble average of the center irradiance value for both models when $\sigma_R^2 = 0.18$.

approach. For example, this is strictly a far-field approximation and does not account for (beam director) aperture obscuration. Though not explored here, other trial solutions (non-Gaussian), e.g., the Zernike polynomial expansion, for beam profile could be explored in future efforts. It is also worth noting that a vectorial variational approach ought to be feasible, where similar methodologies are applied to the full vectorial wave equation (1). Another avenue for future work would be to include thermal effects due to atmospheric heating by the laser beam in order to study the *thermal blooming* issue, especially within a control loop of a beam control system. Finally, it would be useful to complete a more formal comparison study of this VSL to other existing scaling laws, effectively extending the work done by Bingham et al. [29].

## ACKNOWLEDGMENTS

The authors of this article would like to thank the U.S. Air Force Office of Scientific Research (AFOSR) Computational Mathematics program for providing funding for this project through project number 16RDCOR347, and to thank the Universities Space Research Association (USRA) for their funding and support through the Air Force Research Laboratory (AFRL) Scholars Program. Additionally, the authors wish to express gratitude to Prof. Olivier Pinaud of the Mathematics Department at Colorado State University, Dr. Laurence Keefe, NRC Senior Research Associate at the AFRL Directed Energy Directorate Laser Division (now with Zebara LLC), and Dr. Sami Shakir, Senior Scientist at Tau Technologies, for their impactful advise and suggestions, all of which substantially helped the progress this project.

**Table 8.** The relative error of the beam center coordinates and the center irradiance for the asymmetrical initial condition.

| $\sigma_R^2$ | $x$-coord. | $y$-coord. | center irradiance |
|---|---|---|---|
| 0.046 | $8.66 \cdot 10^{-3}$ | $2.08 \cdot 10^{-2}$ | $3.41 \cdot 10^{-2}$ |
| 0.18 | $1.93 \cdot 10^{-2}$ | $4.24 \cdot 10^{-2}$ | $1.57 \cdot 10^{-1}$ |
| 0.41 | $2.82 \cdot 10^{-2}$ | $7.15 \cdot 10^{-2}$ | $2.83 \cdot 10^{-1}$ |

## REFERENCES

1. A. N. Kolmogorov, "*The local structure of turbulence in incompressible viscous fluid for very large Reynolds numbers*," Proc. USSR Acad. Sci. **30**, 299–303 (1941).
2. U. Frisch, *Turbulence: The legacy of A. N. Kolmogorov* (Cambridge University Press, 1995).
3. L. C. Andrews and R. L. Phillips, *Laser Beam Propagation Through Random Media*, vol. 152 (SPIE Press, Bellingham, WA, 2005).
4. J. W. Goodman, *Statistical Optics* (John Wiley & Sons, 2015).
5. F. Wang, X. Liu, and Y. Cai, "*Propagation of partially coherent beam in turbulent atmosphere: a review*," Prog. EM Res. **150**, 123–143 (2015).
6. J. Isaacs and P. Spangle, "*The effect of laser noise on the propagation of laser radiation in dispersive and nonlinear media*," in *Laser Communication and Propagation through the Atmosphere and Oceans VII*, vol. 10770 (International Society for Optics and Photonics, 2018).
7. R. Noriega-Manez and J. Gutierrez-Vega, "*Rytov theory for Helmholtz-Gauss beams in turbulent atmosphere*," Opt. Exp. **15**, 16328–16341 (2007).
8. W. Wanjun, W. Zhensen, S. Qingchao, and B. Lu, "*Propagation of Bessel Gaussian beams through non-Kolmogorov turbulence based on Rytov theory*," Opt. Express **26**, 21712–21724 (2018).
9. L. C. Andrews, M. A. Al-Habash, C. Y. Hopen, and R. L. Phillips, "*Theory of optical scintillation: Gaussian-beam wave model*," Waves Random Media **11**, 271–291 (2001).
10. L. C. Andrews, R. L. Phillips, R. J. Sasiela, and R. R. Parenti, "*Strehl ratio and scintillation theory for uplink Gaussian-beam waves: beam wander effects*," Opt. Eng. **45**, 076001 (2006).
11. D. C. Smith, "*High-power laser propagation: thermal blooming*," Proc. IEEE **65**, 1679–1714 (1977).
12. B. Akers and J. Reeger, "*Numerical simulation of thermal blooming with laser-induced convection*," J. Em. Waves Apps. **33**, 96–106 (2019).
13. H. T. Yura, "*Atmospheric turbulence induced laser beam spread*," Appl. Opt. **10** (1971).
14. M. Whiteley and E. Magee, "*Scaling for High Energy Laser and Relay Engagement (SHaRE) A toolbox for Propagation and Beam Control Effects Modeling User's Guide Version 2010a.957*," Tech. rep., MZA Associates Corporation (2010). Not publicly released.
15. V. Kitsios, J. Frederiksen, and M. Zidikheri, "*Subgrid model with scaling laws for atmospheric simulations*," J. Atmospheric Sci. **69** (2012).
16. N. Van Zandt, S. Fiorino, and K. Keefer, "*Enhanced, fast-running scaling law model of thermal blooming and turbulence effects on high energy laser propagation*," Opt. Express **21**, 14789–14798 (2013).
17. S. Shakir, T. Dolash, M. Spencer, R. Berdine, D. Cargill, and R. Carreras, "*General wave optics propagation scaling law*," JOSA A **33**, 2477–2484 (2016).
18. C. Fox, *An Introduction to the Calculus of Variations* (Dover Publications Inc., New York, 1987).
19. S. Nagaraj, J. Grosek, S. Petrides, L. Demkowicz, and J. Mora, "*A 3D DPG Maxwell Approach to Nonlinear Raman Gain in Fiber Laser Amplifiers*," J. Comput. Physics: X **2**, 100002 (2019).
20. A. Hemming, N. Simakov, J. Haub, and A. Carter, "*A review of recent progress in holmium-doped silica fibre sources*," Opt. Fiber Technol. **20**, 621–630 (2014).

21. D. Anderson, "*Variational approach to nonlinear pulse propagation in optical fibers*," Phys. review A **27**, 3135 (1983).
22. D. Anderson, M. Lisak, and T. Reichel, "*Approximate analytical approaches to nonlinear pulse propagation in optical fibers: A comparison*," Phys. Rev. A **38**, 1618 (1988).
23. D. Anderson and M. Lisak, "*A variational approach to the nonlinear Schrödinger equation*," Phys. Scripta **1996**, 69 (1996).
24. G. Pichot, "*Algorithms for Gaussian Random Field Generation*," Tech. rep., Project-Team SERENA (2017).
25. G. Strang, "*On the Construction and Comparison of Difference Schemes*," SIAM J. Numer. Analysis **5**, 506–517 (1968).
26. S. MacNamara and G. Strang, "*Operator Splitting*," in *Splitting Methods in Communications, Imaging, Science, and Engineering,* R. Glowinski, S. J. Stanley, and W. Yin, eds. (Springer International Publishing, 2016).
27. M. Roggemann, B. Welsh, D. Montera, and T. Rhoadarmer, "Method for simulating atmospheric turbulence phase effects for multiple time slices and anisoplanatic conditions," OSA Appl. Opt. **34**, 4037–4051 (1991).
28. J. Schmidt, *Num. Sim. of Optical Wave Propagation* (SPIE, 2010).
29. S. Bingham, M. Spencer, N. Van Zandt, and M. Cooper, "*Wave-optics comparisons to a scaling law formulation*," in *Unconventional and Indirect Imaging, Image Reconstruction, and Wavefront Sensing 2018,* (International Society for Optics and Photonics, 2018).